Electromagnetic Torque Analysis of SRM 12/8 by Rotor/Stator Pole Angle

Dinh Bui Minh
School of Electrical Engineering
Hanoi University of Science and Technology
Hanoi, Vietnam

Linh Dinh Hai
School of Electrical Engineering
Hanoi University of Science and Technology and
College of Electromechanical and Civil Engineering
Vietnam National University of Forestry
Hanoi, Vietnam

Tuan Le Anh
Hanoi University of Industry
Hanoi, Vietnam

Vuong Dang Quoc
School of Electrical Engineering
Hanoi University of Science and Technology
Hanoi, Vietnam

.

Abstract—This paper presents the harmonic torque reduction by the different rotor pole angles of a three-phase 12/8 switched reluctance motor via an analytical model and simulation method. Improving torque performance by stator and rotor angles was applied for three-phase switched reluctance motor at stator pole/rotor pole ratios of 6/4, 8/12, 18/12, and 24/18. The average torque and the torque ripple effect by stator and rotor pole embrace have been recently studied in many projects. Due to the fact that leakage flux, flux density, and inductance are affected by the stator and rotor pole angles non-linear and linear leakage flux curves occur. Many stator and rotor pole angle combinations for the three-phase switched reluctance motor have already been done via a finite element method. In this paper, turn-on and turn-off angles will be figured based on stator and rotor pole embraces.

Keywords-Switched Reluctance Motor (SRM); pole arcs; torque; Finite Element Method (FEM)

I. INTRODUCTION

Nowadays, the Switched Reluctance Motor (SRM) is considered as the most appropriate candidate to drive small scale electric vehicles due to advantages such as its simple construction, wide constant power regions, and effective torque speed characteristics. The SRMs have been applied in various fields [1-5]. A convenient design of the SRM has a significant importance for an efficient performance of the motor. Some design parameters must be considered such as the number of phases, stator pole arc, air gap thickness, and other SRM geometry elements. The effect of the SRM geometry on the motor performance has been examined thoroughly. In [6], the influence of pole embrace has been investigated on the performance of the SRM by the Finite Element Method (FEM) with stator and rotor pole embraces changing from 0.2 to 0.5. According to the highest average torque and lowest torque ripple, the proper pole embraces have been selected for the optimum design of the SRM [7-9].

II. ELECTROMAGNETIC TORQUE ANALYSIS

The rotor and stator pole arc angles are a critical part in the design of the SRMs. The rotor pole arc (β_r) must be equal or greater than the stator pole arc (β_s), because the number of rotor poles is less than the number of stator poles ($\beta_s \leq \beta_r$). When the βs is smaller than the step angle, then none of the phases can have rising inductance slope. The rotor pole angle should be greater than the sum of stator and rotor pole arcs [10]:

$$\beta_r \geq \beta_s; \quad \beta_r + \beta_s < \frac{360^0}{N_r}; \quad \min(\beta_r, \beta_s) \geq \frac{360^0}{m.N_r} \quad (1)$$

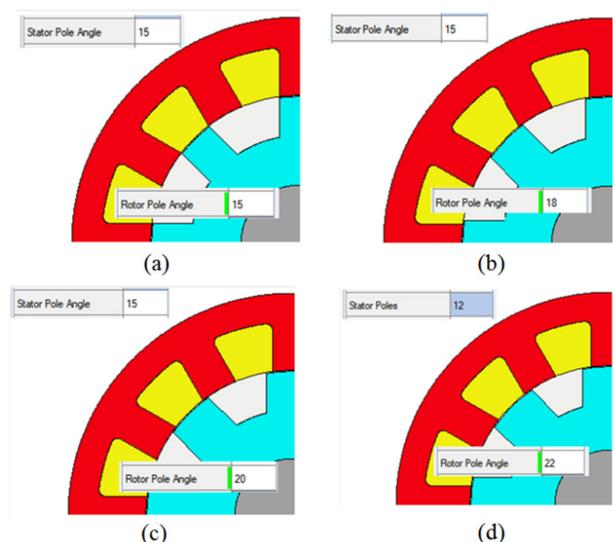Fig. 1.   Cross-section of a three-phase SRM 12/8 β_r equal to (a) 15^0, (b) 18^0, (c) 20^0, (d) 22^0 for β_s=15^0, 15^0, 15^0, and 12^0 respectively.

Corresponding author: Dinh Bui Minh (dinh.buiminh@hust.edu.vn)

The initial size L is estimated from the output power and torque with speed of 1500rpm. With an initial assumption for the L and with respect to the average torque proportionality with LD^2, the values of L and D have been calculated via the analytical method. The three phase SRMs 12/8 with rotor angle $(15^0 \div 22^0)$ are listed in Table I.

TABLE I.   TECHNICAL PARAMETERS OF SRM 12/8

Technical Parameters	Value	Units
Stator poles	12	
Stator pole angle	15	degrees
Stator lam dia	140	mm
Stator bore	90	mm
Stator pole depth	15	mm
Stator duct layers	2	
Rotor pole angle	15, 18, 20, 22	degrees
Rotor slot depth	11	mm
Airgap	0.3	mm
Number strands in hand	9	
Phases	3	
Turns per phase	12	
Power	1200	W
Speed	1500	rpm
Torque	12	N.m
Rotor pole τ_r (360/Nr=360/8)	45	degrees
Stator pole τ_r (360/Ns=360/12)	30	degrees

The static torque curves (T_c) have been implemented with FEM with current ranging from 0 to 50A depending on the rotor angle, i.e.:

$$T_c = \frac{1}{2} i^2 \frac{dL(\theta, i)}{d\theta} \quad (2)$$

The rotor embrace ratio a_s and stator embrace ratio a_r are determined by:

$$a_s = \frac{\beta_s}{\tau_s}, \quad a_r = \frac{\beta_r}{\tau_r} \quad (3)$$

In order to maximize the static electromagnetic torque, the stator embrace angle values of 0.45, 0.5, 0.55, 0.6, or 13.5^0, 15^0, 16.5^0, 18^0 have been applied to the finite element simulation to get the static torque, and the rotor angle is verified from 0 to 45^0 as shown in Figure 2.
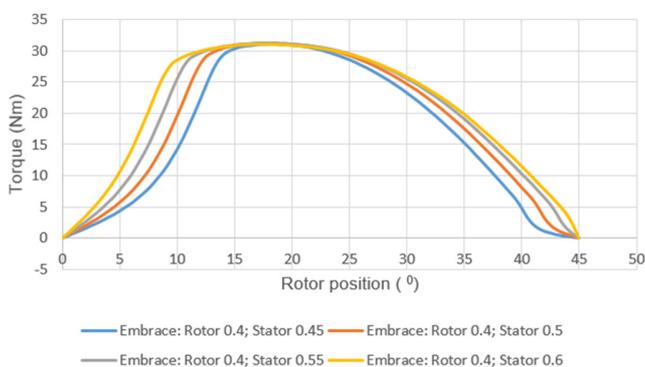
Fig. 2.   The static torque curves and rotor position stator pole embrace for rotor embrace of 0.4.

The static torque curves have been also evaluated with rotor embrace ratio of 0.5 and stator pole embrace values of 0.45, 0.5, 0.55, 0.6 or 13.5^0, 15^0, 16.5^0, 18^0. The stator pole embrace is changed from 0.45 to 0.6 with 0.05 steps for constant rotor pole embrace of 0.5 as shown in Figure 3. It is obtained that the combination of 0.40 rotor pole and 0.5 stator pole embraces produces the highest peak output torque which is 31.046Nm. Besides, the combination of stator and rotor pole embraces at 0.40 value has the minimum output torque which is 30.920Nm.
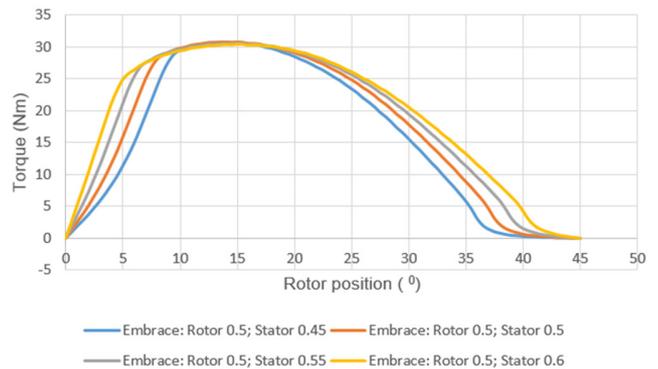
Fig. 3.   The static torque curves and rotor position stator pole embrace for rotor embrace of 0.5.

The stator pole embrace is changed from 0.45 to 0.6 with steps of 0.05 for a constant of 0.40 rotor pole embrace depicted in Figure 3. It is seen that the combination of 0.5 rotor pole and 0.50 stator pole embraces produces the highest peak output torque which is 31.191Nm. In the same way, the combination of stator pole embrace and 0.50 rotor pole embrace has the minimum output torque which is 31.094Nm. As can be seen from the results, while the highest output torque is obtained by the combination of 0.40 rotor pole and 0.5 stator pole embraces, the lowest output torque is obtained by the combination of 0.6 rotor pole and 0.6 stator pole embraces. According to these combinations, the optimum values of pole arcs stator/rotor can be selected for better motor design. The average torque is calculated and the best combination of stator and rotor pole embrace can be selected for optimum analysis. The results on the effect of pole embrace are given in Figure 4 for different combinations of the stator and rotor pole embraces.
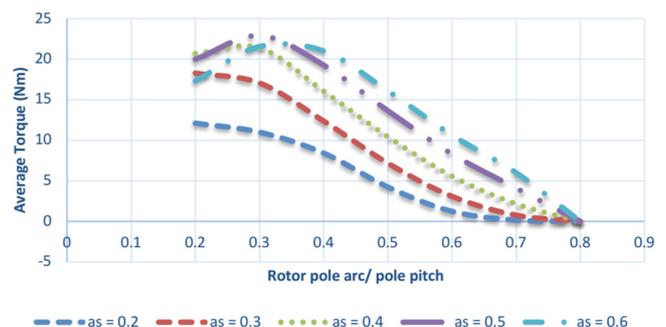
Fig. 4.   Average Torque vs rotor embrace.

Figure 5 shows the average torque and torque ripple, and the embrace stator for various values of the embrace rotor. The average torque is maximum or on top of the curve (a_s=0.5) at rotor pole arc a_r=0.3. With the 4 rotor poles and 6 SRM stator poles, the rotor/stator pitches are 45/30 degrees. Thus, the rotor embrace a_r=0.3 is 30 mechanical degrees and the stator embrace is a_r=0.5. This means that the rotor pole angle and stator angle have the same value of 15 degrees. The electromagnetic torques with different rotor and stator embraces are presented in Table II. From those results, the best combination of a_s=0.3 and a_r=0.5 is selected to verify the dynamic torque performance.
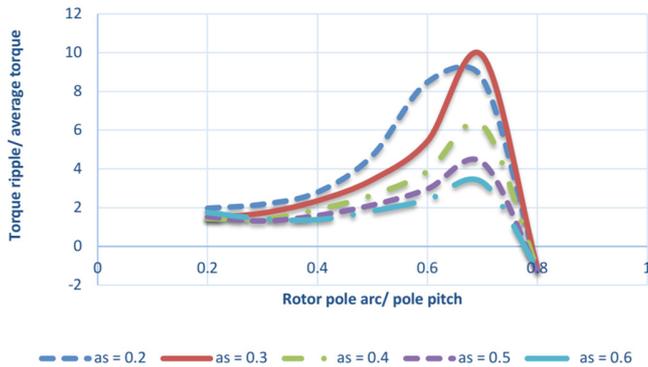

Fig. 5.   Torque ripple/average torque rate vs rotor embrace.

TABLE II.   AVERAGE TORQUE (Nm).

a_r	a_s=0.2	a_s=0.3	a_s=0.4	a_s=0.5	a_s=0.6
0.2	12.09608	18.2667	20.69018	19.97587	17.31098
0.3	10.9917	17.04873	21.39854	22.89821	21.54776
0.4	8.411142	12.35922	16.03515	19.25603	21.00559
0.5	4.228949	7.167675	10.4344	13.63371	16.0756
0.6	1.233799	3.079451	5.558719	8.299413	10.63121
0.7	0.150363	0.761016	2.154871	4.085025	5.991545

III.   DYNAMIC SIMULATION AND EXPERIMENTAL RESULTS

The finite element model has been presented to validate the dynamic torque of 1500rpm and phase current *I*=50A. The turn on and turn off angles are determined in (4). The torque curve plot is depicted in Figure 6. The torque ripple ranges from 5 to 9N.m.

$$\begin{cases} T_{on} = \theta_{on} = -(\beta_{r-}\beta_s) \\ T_{off} = \theta_{off} = -(\beta_{r-}\beta_s) + \frac{\pi}{N_r} \end{cases} \quad (4)$$

The dynamic torque and efficiency with different rotor and stator angles are compared in Table III. The SRM 12/8 with β_s=15^0, β_r=18^0 is the maximum average torque and minimum torque ripple. The harmonic torque of SRM 12/8 is classified with multiples of 3 oders such as 3th, 6th, 9th, 12th and 15th because the SRM 12/8 has 3 phases in stator and 4 coils/phase (Figure 7). The total torque of SRM 12/8 can be calculated by 3th, 6th, 9th, 12th and 15th. The 3th harmonic component is still significant on the torque ripple. Therefore, this study will investigate different stator and rotor embrace angles on the harmonic torque and total torque.
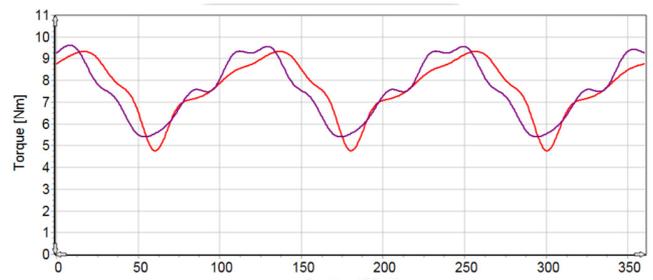

Fig. 6.   Dynamic torque curve at 1500rpm.

TABLE III.   SRM 12/8 ELECTROMAGNETIC PERFORMANCE COMPARISON

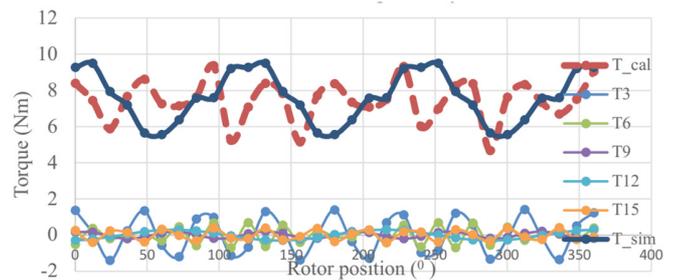| Parameters	Unit	15^0/15^0	15^0/16.5^0	15^0/18^0	15^0/20^0
Maximum possible torque	Nm	8.466	8.6722	8.6466	8.5649
Average torque	Nm	7.642	8.0111	8.1424	7.9893
Average torque	Nm	7.496	7.9467	8.159	8.1269
Torque ripple	Nm	4.223	1.9376	1.9682	2.4121
Torque ripple [%]	%	57.93	23.812	23.958	29.622
Electromagnetic power	W	916.1	1022.5	1032.4	1023.3
Input power	W	1092	1198.8	1207.6	1195.1
Output power	W	872.7	976.22	985.65	976.53
Total losses (on load)	W	219.4	222.55	221.99	218.59
System efficiency	%	79.91	81.435	81.618	81.71
Shaft torque	Nm	6.945	7.7685	7.8435	7.771

Fig. 7.   Harmonic torque.

The dynamic torque test bench installation for SRM 12/8 and permanent magnet generator in the torque transduce is shown in Figure 8. The torque sensor TM300 is connected to PC to get the data during testing.

Fig. 8.   Dynamic torque test bench.

The speed and torque values with different time steps are presented in Figure 9. In the time interval from 1s to 5s, the

speed and torque are very stablized and vary trivially. However, torque ripple appears in the begining time (0.02s). These values are also recorded in starting stage and constant speed. The dynamic torque with different rotor positions is shown in Figure 10. The values on the torque at stator 15 and rotor 22 reach approximately 10Nm.
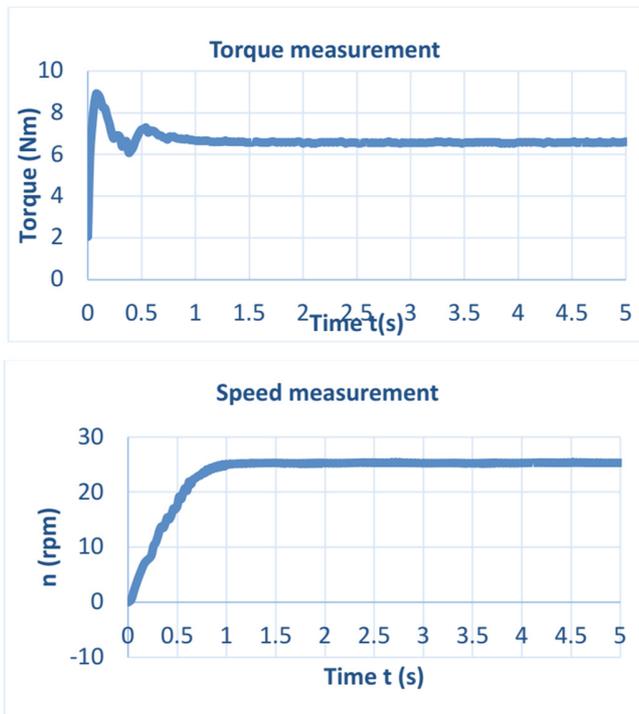

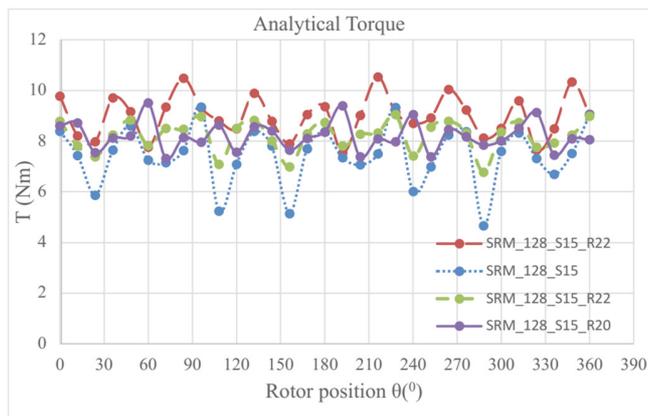Fig. 9.   Dynamic speed (top) and torque (bottom).

Fig. 10.   Dynamic torque with differnt rotor positions.

IV. CONCLUSION

The current paper has developed stator and rotor embrace/pitch influenced on the average torque and torque ripples via FEM [10, 11]. For high speed of the SRM, the control method is single voltage or current pulse because the magnetic circuit is saturated. Thus, it is difficult for chopping current to apply and the phase current cannot reach reference values. The electromagnetic design will help improving torque and current controller. The static torque curves have been also evaluated by the FEM. This paper also demonstrates a method to improve and design the SRMs in practice.

REFERENCES

[1] R. M. Azhagar and A. Kavitha, "Effect of rotor geometry on Peak and Average Torque of direct drive External-Rotor Synchronous Reluctance Motor (Ex-R SynRM) in comparison with Switched Reluctance Motor for low speed domestic application," in *2017 IEEE International Magnetics Conference (INTERMAG)*, Dublin, UK, Apr. 2017, pp. 1–2, https://doi.org/10.1109/INTMAG.2017.8007641.

[2] J. Han, B. Ge, K. Zhang, Y. Wang, and C. Wang, "Influence of Control and Structure Parameters on the Starting Performance of a 12/8 Pole Switched Reluctance Motor," *Energies*, vol. 13, no. 14, Jan. 2020, Art. no. 3744, https://doi.org/10.3390/en13143744.

[3] N. K. Sheth and K. R. Rajagopal, "Optimum pole arcs for a switched reluctance motor for higher torque with reduced ripple," *IEEE Transactions on Magnetics*, vol. 39, no. 5, pp. 3214–3216, Sep. 2003, https://doi.org/10.1109/TMAG.2003.816151.

[4] M. Yildirim and H. Kurum, "Influence of Poles Embrace on In-Wheel Switched Reluctance Motor Design," in *2018 IEEE 18th International Power Electronics and Motion Control Conference (PEMC)*, Budapest, Hungary, Aug. 2018, pp. 562–567, https://doi.org/10.1109/EPEPEMC.2018.8521859.

[5] A. Tap, L. Xheladini, T. Asan, M. Imeryuz, M. Yilmaz, and L. T. Ergene, "Effects of the rotor design parameters on the torque production of a PMaSynRM for washing machine applications," in *2017 International Conference on Optimization of Electrical and Electronic Equipment (OPTIM) 2017 Intl Aegean Conference on Electrical Machines and Power Electronics (ACEMP)*, Brasov, Romania, May 2017, pp. 370–375, https://doi.org/10.1109/OPTIM.2017.7974998.

[6] R. Krishnan, *Switched Reluctance Motor Drives: Modeling, Simulation, Analysis, Design, and Applications*, 1st ed. Boca Raton, FL, USA: CRC Press, 2001.

[7] Z. Yueying, Y. Chuantian, Y. Yuan, W. Weiyan, and Z. Chengwen, "Design and optimisation of an In-wheel switched reluctance motor for electric vehicles," *IET Intelligent Transport Systems*, vol. 13, no. 1, Jan. 2019.

[8] A. Siadatan, M. Roohisankestani, and S. Farhangian, "Design and Simulation of a new Switched Reluctance Motor with changes in the shape of stator and rotor in order to reduce torque ripple and comparison with the conventional motor," in *2018 International Symposium on Power Electronics, Electrical Drives, Automation and Motion (SPEEDAM)*, Amalfi, Italy, Jun. 2018, pp. 353–358, https://doi.org/10.1109/SPEEDAM.2018.8445245.

[9] O. M. Al-Barbarawi, "Improving Performance of the Braking Process, and Analysis Torque-Speed Characteristics of the Induction Motor," *Engineering, Technology & Applied Science Research*, vol. 8, no. 6, pp. 3585–3591, Dec. 2018, https://doi.org/10.48084/etasr.2325.

[10] V. D. Quoc, "Robust Correction Procedure for Accurate Thin Shell Models via a Perturbation Technique," *Engineering, Technology & Applied Science Research*, vol. 10, no. 3, pp. 5832–5836, Jun. 2020, https://doi.org/10.48084/etasr.3615.

[11] V. D. Quoc, "Accurate Magnetic Shell Approximations with Magnetostatic Finite Element Formulations by a Subdomain Approach," *Engineering, Technology & Applied Science Research*, vol. 10, no. 4, pp. 5953–5957, Aug. 2020, https://doi.org/10.48084/etasr.3678.